

Supramolecular Polymers

How to cite:

International Edition: doi.org/10.1002/anie.202214997

German Edition: doi.org/10.1002/ange.202214997

Heterocyclic Chromophore Amphiphiles and their Supramolecular Polymerization

Luka Đorđević, Hiroaki Sai, Yang Yang, Nicholas A. Sather, Liam C. Palmer, and Samuel I. Stupp*

Abstract: Supramolecular polymerization of π -conjugated amphiphiles in water is an attractive approach to create functional nanostructures. Here, we report on the synthesis, optoelectronic and electrochemical properties, aqueous supramolecular polymerization, and conductivity of polycyclic aromatic dicarboximide amphiphiles. The chemical structure of the model perylene monoimide amphiphile was modified with heterocycles, essentially substituting one fused benzene ring with thiophene, pyridine or pyrrole rings. All the heterocycle-containing monomers investigated underwent supramolecular polymerization in water. Large changes to the monomeric molecular dipole moments led to nanostructures with low electrical conductivity due to diminished interactions. Although the substitution of benzene with thiophene did not notably change the monomer dipole moment, it led to crystalline nanoribbons with 20-fold higher electrical conductivity, due to enhanced dispersion interactions as a result of the presence of sulfur atoms.

Introduction

Electronically active and ordered assemblies of molecules found in biological systems provide excellent inspiration for the design of soft energy materials using supramolecular polymerization of π -conjugated molecules.^[1] Over the years, these have evolved to be highly functional as media for exciton transport in artificial photosynthesis, sensing, and supramolecular electronics.^[2] In this context it is useful to study the conductivity of self-assembled one-dimensional π - π stacked nanostructures and thus improve charge transport and optimize energy devices.^[3] While much progress has been made in preparing supramolecular conductive materials in organic solvents,^[3a,4] there is great interest in developing functional materials in aqueous solutions and hydrogels for “green” chemistry.^[5] Development of such materials requires functionalization of π -electron systems with water-solubilizing groups that can also help direct self-assembly and create supramolecular polymers. For this

purpose, oligoethylene glycol chains and amino acids were employed to functionalize oligothiophenes,^[6] diketopyrrolopyrroles,^[7] naphthalene imides,^[8] and perylene diimides.^[9]

Our group has developed a supramolecular chromophore amphiphile system based on a hydrophobic perylene monoimide (PMI) core linked, through an alkyl chain, to a water-solubilizing carboxylate group.^[10] This compound was found to self-assemble in water into nanoribbons, through dipolar interactions and π - π stacking, and exhibit a crystalline packing arrangement under charge screening conditions. Additional previous work showed that a five-carbon alkyl chain (PMI-L₅), between the aromatic core and hydrophilic charged group, led to optimal molecular packing.^[10b] Furthermore, chemical modifications at the 9-position of the perylene core had a strong impact on the self-assembly of PMI derivatives,^[10f] mostly due to changes to the dipole moment of the monomers that lead to changes in dipolar interactions during supramolecular polymerization.^[10c-h] For

[*] Dr. L. Đorđević, Dr. H. Sai, Dr. Y. Yang, Dr. L. C. Palmer, Prof. Dr. S. I. Stupp
 Center for Bio-Inspired Energy Science, Northwestern University
 Evanston, IL 60208 (USA)
 E-mail: s-stupp@northwestern.edu
 Dr. L. Đorđević, Dr. L. C. Palmer, Prof. Dr. S. I. Stupp
 Department of Chemistry, Northwestern University
 Evanston, IL 60208 (USA)
 Dr. L. Đorđević
 Present address: Department of Chemical Sciences, University of Padova
 35131 Padova (Italy)
 Dr. H. Sai, Dr. Y. Yang, Dr. N. A. Sather, Dr. L. C. Palmer, Prof. Dr. S. I. Stupp
 Simpson Querrey Institute for BioNanotechnology, Northwestern University
 Chicago, IL 60611 (USA)

Dr. N. A. Sather, Prof. Dr. S. I. Stupp
 Department of Materials Science and Engineering, Northwestern University
 Evanston, IL 60208 (USA)
 Prof. Dr. S. I. Stupp
 Department of Medicine, Northwestern University
 Chicago, IL 60611 (USA)
 and
 Department of Biomedical Engineering, Northwestern University
 Evanston, IL 60208 (USA)

© 2023 The Authors. Angewandte Chemie International Edition published by Wiley-VCH GmbH. This is an open access article under the terms of the Creative Commons Attribution Non-Commercial License, which permits use, distribution and reproduction in any medium, provided the original work is properly cited and is not used for commercial purposes.

example, introduction of electron-donating substituents (such as amine, alkylamines, methoxy and hydroxy groups) resulted in higher molecular dipole moments and the consequent dipolar interactions led to crystalline nanostructures.^[10c-i]

We report here the synthesis of heterocycle-containing amphiphilic polycyclic aromatic dicarboximides (PADIs) and investigate their self-assembly into crystalline supramolecular polymers. We reasoned that replacing one of the fused benzene rings with heterocycles in the canonical PMI would be a good strategy to modulate their optoelectronic^[11] and self-assembling behavior. Heteroatom doping of polycyclic aromatic hydrocarbons, through various synthetic routes, has emerged as a useful approach to tailor their band gaps, redox properties, crystallization, aromaticity, and chemical stability.^[12] While introducing heteroatoms in monomeric structures has been employed to direct self-assembly,^[13] much less is known about systematically probing the effect of heterocycles on supramolecular polymerization of chromophores. The optoelectronic and electrochemical properties of the monomeric PADIs were studied in organic solutions, while their supramolecular self-assembly was studied in aqueous media. The formation of supramolecular polymers was studied through a combination of absorption and emission spectroscopies, various microscopic techniques, and X-ray scattering. We also explore the effect of heteroatom-substitution on the conductivity of these supramolecular polymers, both in bulk and at the nanoscale.

Results and Discussion

Molecular design and synthesis

Based on the chemical structures and estimated dipole moments depicted in Figure 1, we reasoned that replacing a fused benzene ring of PMI-L₅ (**1**) with heterocycles (i.e., modifying positions 8 and 9 of the perylene core) would lead to changes in the optoelectronic and redox properties of the monomers. Small changes, like in the case of benzene-to-thiophene substitution in S-PADI-L₅ (**2**), would allow us to study the effect of the heteroatom-substituted ring on polymerization and the properties of the final material. In contrast, larger changes in the electron-density of the aromatic core are more likely to affect the supramolecular polymerization and could make it harder to discern short-range interactions due to introduction of heterocycles. In the latter case, substitution of a fused benzene ring with either an electron-deficient (pyridine) or electron-rich (pyrrole) heterocycles, would yield N_{pyridine}-PADI-L₅ (**3**) and N_{pyrrole}-PADI-L₅ (**4**). We confirmed our initial hypothesis by performing density functional theory (DFT) analysis and compared the calculated dipole moments (μ), the electrostatic surface potentials (ESP), and the frontier molecular orbitals (see Figure 1 and Supporting Information, Section 7 for computational details). Indeed, comparing the molecules to the canonical PMI-L₅ (**1**), thiophene substitution (**2**) for the fused benzene ring leads to little change in molecular

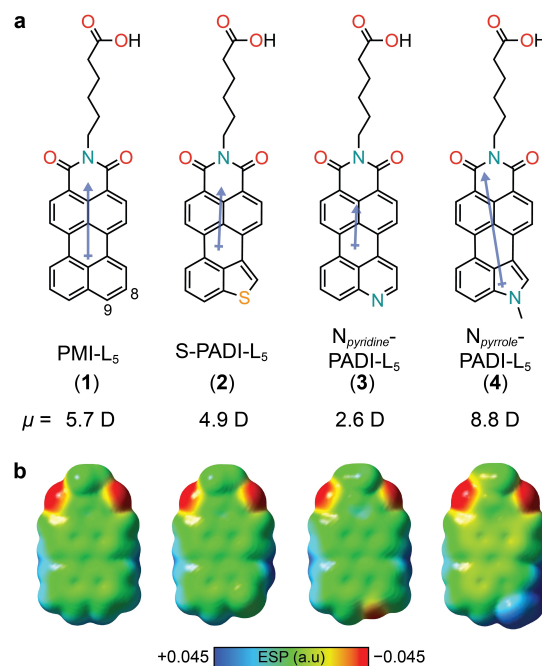
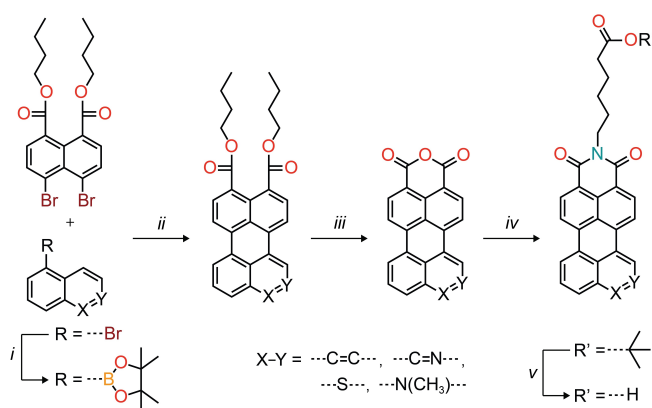


Figure 1. a) Chemical structures of the chromophore amphiphiles discussed in this work, along with their calculated dipole moments (blue arrows indicate the direction, while their values are below the structures) and their b) calculated electrostatic surface potentials (ESP). The carboxyalkyl chain was replaced with a methyl group in the DFT calculations.

properties: the dipole moment slightly decreases from $\mu = 5.7$ D to $\mu = 4.9$ D, there is a similar charge distribution (with the notable presence of a bigger sulfur atomic radius), and similar orbital energies are observed. Heterocycle substitution in pyridine-containing molecule **3** shows a decrease of the dipole moment ($\mu = 2.6$ D), a decrease of electron density, and a downward shift of the frontier energy orbitals. The opposite trend is observed for pyrrole-substituted molecule **4** ($\mu = 8.8$ D), which showed an increase of electron density, and an upward shift of the frontier energy orbitals.

As depicted in Scheme 1 (and Scheme S1), we sought to take advantage of the palladium (Pd)-catalyzed annulation reaction between naphthalene dicarboximide (**S2**) and different (hetero)aromatic substrates.^[11a,b,14] We first attempted the Pd-catalyzed C–C bonds formation cascade reactions between the 4,5-dibromonaphthalene-1,8-dicarboximide (**S16**), carrying a *tert*-butyl hexanoate group in the imide position, and 1-naphthaleneboronic acid pinacol ester (**S3**).^[11a] The successful progress of the reaction was evident by the appearance of a dark orange-red product, but its purification was challenging due to the propensity of the sterically unhindered PMIs to aggregate. We therefore reasoned that the synthesis, and subsequent purification, would be easier by first preparing the perylene diester and then proceeding with the imidization reaction (**S4**). The Pd-catalyzed annulation reaction between 4,5-dibromonaphthalene-1,8-di(*n*-butylcarboxylate) (**S2**) and 1-naphthaleneboronic acid pinacol ester (**S3**), indeed gave pure perylene diester (**S4**) after column chromatography in excellent yield



(98%). The perylene diester was then subjected to a dehydration reaction under strongly acidic conditions to form the perylene monoanhydride. Following the imidization reaction, with *tert*-butyl 6-aminohexanoate in the presence of base, we obtained *tert*-butyl protected PMI-L₅ (**S5**), which could be easily deprotected with trifluoroacetic acid to afford the corresponding carboxylic acid (PMI-L₅, **1**). It is important to note that this route yields PMI-L₅ compound in high purity (>99 %, Supporting Information, Figure S1) and scalable quantities: previous synthetic protocols afforded methyl ester PMI-L₅ that required additional purification by recycling gel permeation chromatography on a 50 mg scale before the final deprotection.^[10e,15]

The other three new heteroaromatic compounds were prepared using the same synthetic approach, by substituting the 1-naphthaleneboronic acid pinacol ester (**S3**) with the appropriate (hetero)aromatic substrate (**S6**, **S9** or **S13**). By using tris(dibenzylideneacetone)dipalladium(0) as catalyst, tricyclohexylphosphine as ligand, K_2CO_3 as base, the polycyclic aromatic diesters **S7** and **S14** could be prepared in very good yields (84–89%). However, the electron-poor nature of the quinoline **S9** precursor reduced the reaction yields in the synthesis of $N_{pyridine}$ polycyclic aromatic diester (**S10**). Using higher temperatures (180 °C in *o*-dichlorobenzene) and longer reaction times (48 h instead of 24 h), naphthalene diester (**S2**) and 5-quinolineboronic acid pinacol ester (**S9**) yielded the annulated product **S10** in sufficient yield (20 %) for the following reactions. The subsequent dehydration, imidization and deprotection reactions were performed as outlined earlier and gave all three of the desired PADI compounds (**2**, **3** and **4**). Compounds **1–4** were unambiguously characterized by NMR spectroscopy and high-resolution mass spectrometry (Supporting Information Section 4), and for S-PADI-L₅ (**2**) the single-crystal

X-ray structure^[16] was resolved (Supporting Information Section 10).

Photophysical and electrochemical properties of monomers

The effect of heterocycle structure on properties of the chromophore monomers was first examined spectroscopically by acquiring their absorption and emission spectra (Figure 2a, 5 μM in dimethylsulfoxide, DMSO). The model PMI-L₅ (**1**) has the lowest energy electronic transition at 505 nm and the substitution of a fused benzene ring by thiophene (S-PADI-L₅, **2**) causes little change to the absorption spectra (λ_{max} = 498 nm), which is expected based on the computational work described above. Introduction of the electron-poor $N_{pyridine}$ -PADI-L₅ (**3**) or electron-rich $N_{pyrrole}$ -PADI-L₅ (**4**), nitrogen-containing rings leads to a shift of the absorption peaks, with λ_{max} = 486 nm and λ_{max} = 555 nm, respectively. We attribute these shifts to changes in the electron densities caused by the introduction of heterocycles. The fluorescence spectra follow the same trend

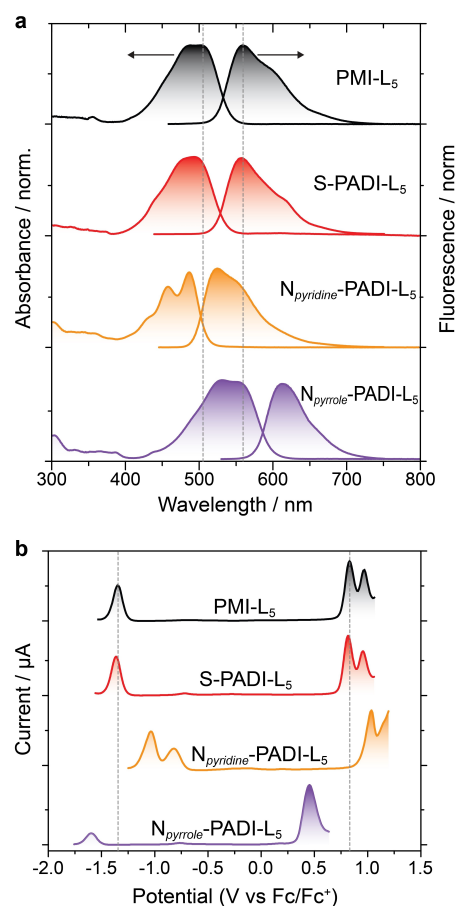


Figure 2. Photophysical and electrochemical properties of PADI monomers in organic solutions. a) Absorption and emission spectra ($\approx 5 \mu M$ in DMSO) and b) differential pulse voltammograms ($\approx 1 mM$ in DMF, TBAPF₆ 100 mM, ferrocene used as internal standard and referenced to zero). The dotted grey lines are guides for comparison with model PMI-L₅.

observed for the absorption spectroscopy (unchanged emission for molecule **2**, blue-shifted emission for **3** and red-shifted emission for **4**). The PADIs possess fluorescence quantum yields (65–85 %) and display Stokes shifts of 38–59 nm, which are relatively small in a polar solvent (DMSO) and are expected for such rigid π -scaffolds.^[14b,e]

The electrochemical properties were determined by cyclic voltammetry (CV) (Supporting Information, Figures S42–S45) and, since the oxidation processes were irreversible, differential pulse voltammetry (DPV). The DPV traces, depicted in Figure 2b, were used to experimentally determine the energy levels of PADIs (≈ 1 mM in DMF) using the ferrocene/ferrocenium couple as reference. The oxidation potential of canonical PMI-L₅ (**1**) is +0.83 V and its reduction potential is –1.35 V, with a band gap of 2.18 V. In agreement with the optical characterization, S-PADI-L₅ (**2**) energy levels resemble those of model compound **1** ($E_{\text{ox}} = +0.81$ V and $E_{\text{red}} = -1.36$ V, with an electrochemical gap of 2.17 V). The electron-poor nature of the pyridyl ring is reflected in the N_{pyridine}-PADI-L₅ (**3**) molecule with $E_{\text{ox}} = +1.03$ V, being more difficult to oxidize (and easier to reduce, $E_{\text{red}} = -0.82$ V) compared to molecule **1**. The electron-rich N_{pyrrole}-PADI-L₅ (**4**), on the other hand, undergoes easier oxidation ($E_{\text{ox}} = +0.46$ V) and more difficult reduction ($E_{\text{red}} = -1.36$ V). The experimentally determined energy levels are in good agreement with theoretical calculations (Supporting Information, Figure S49).

Aqueous supramolecular polymerization and nanostructure morphology

Having determined the photophysical and redox properties of monomeric PADIs, we proceeded to investigate their self-assembly behavior through supramolecular polymerization. The samples were prepared by suspending solid PADIs in water, followed by deprotonation of the carboxylic acids with one equivalent of NaOH to yield PADI supramolecular polymers in solution (at 12 mM, Supporting Information Figure S54). Since these nanostructures were found to be amorphous (Supporting Information, Figures S55–S58), we then added aq. NaCl (300 mM, 1:5 volume ratio of salt solution to PADI solution) to electrostatically screen repulsive forces among carboxylate groups and promote stacking (final concentration of PADI is 10 mM and NaCl 50 mM) (Supporting Information, Figures S55–S58). The resulting nanostructures were indeed crystalline nanoribbons (except for N_{pyridine}-PADI-L₅ **3**, see discussion below). Finally, the PADI samples were thermally annealed at 95 °C for 1 hour and then slowly cooled^[10h,15] to obtain supramolecular nanostructures closer to thermodynamic equilibrium and avoid formation of kinetically trapped states.^[17] The process of supramolecular self-assembly was also probed by recording absorbance and emission traces at each step of the procedure (Figures S59–S62, Supporting Information). Compared to absorbance traces of their monomeric solutions in DMSO (Figure 2a), aqueous solutions of PADIs show blue-shifted absorption maxima, indicating formation of supramolecular polymers (Support-

ing Information, Figures S59–S62). Charge screening and thermal annealing of PADI samples led to the splitting of the supramolecular polymer peak into a blue-shifted one and a red-shifted one (Figure 3). This observation is consistent with previous reports that assigned the blue-shifted absorption peak to intramolecular (Frenkel) excitons, while the red-shifted peak was attributed to the formation of intermolecular (charge-transfer) excitons.^[18] All the self-assembled polymers therefore show the formation of delocalized excitons. Furthermore, strong fluorescence quenching confirms the presence of supramolecular H-type aggregation (Supporting Information, Figures S59–S62).

The internal degree of order within the supramolecular polymers formed were studied by small- and wide-angle X-ray scattering (SAXS/WAXS) experiments on PADI compounds using synchrotron irradiation. The scattering slopes in the low q regime (Guinier region) of PADI SAXS profiles are –2 (Figure 4a), consistent with a ribbon-like nanostructure morphology. As mentioned above, crystalline peaks are not observed in aqueous solutions without charge screening (Supporting Information, Figures S55–S58). Addition of salt leads to the presence of crystalline Bragg peaks observed in WAXS scans of PADIs **1**, **2** and **4**, while N_{pyridine}-PADI-L₅ (**3**) shows only a broad peak at 1.8 \AA^{-1} indicative of π – π stacking. As expected, annealing PADIs **1**, **2** and **4** solutions result in an increase in the intensity of Bragg peaks (Figure 4b) because of further ordering of monomers within the polymeric assemblies. Crystalline assemblies of **1** show strong Bragg reflections at 0.75 , 1.76 and 1.89 \AA^{-1} ($\pm (20)$, $\pm (02)$, and the $\pm (22)$ reflections),^[10a] while S-PADI-L₅ (**2**) polymers show a similar 2D oblique lattice with strong reflections at 0.71 , 1.66 and 1.89 \AA^{-1} . N_{pyrrole}-PADI-L₅ (**4**) shows clear Bragg reflections at 0.85 , 1.02 , 1.22 , 1.68 and 2.03 \AA^{-1} . A similar pattern to the N_{pyrrole}-PADI-L₅ (**4**) polymers was previously reported for a PMI derivative with

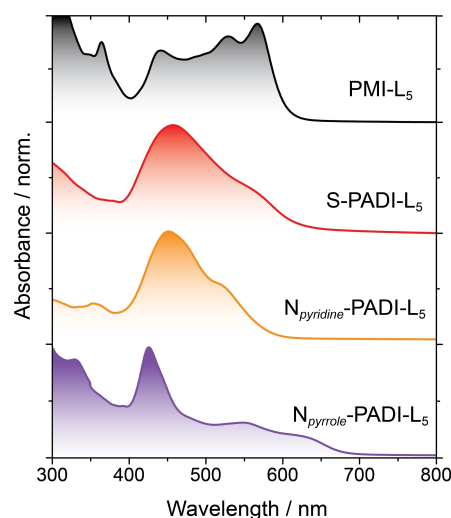


Figure 3. Absorption spectra of polymerized chromophore amphiphiles in water (10 mM PADI with 50 mM aq. NaCl, annealed at 95 °C for 1 hour and then slow-cooled to room temperature).

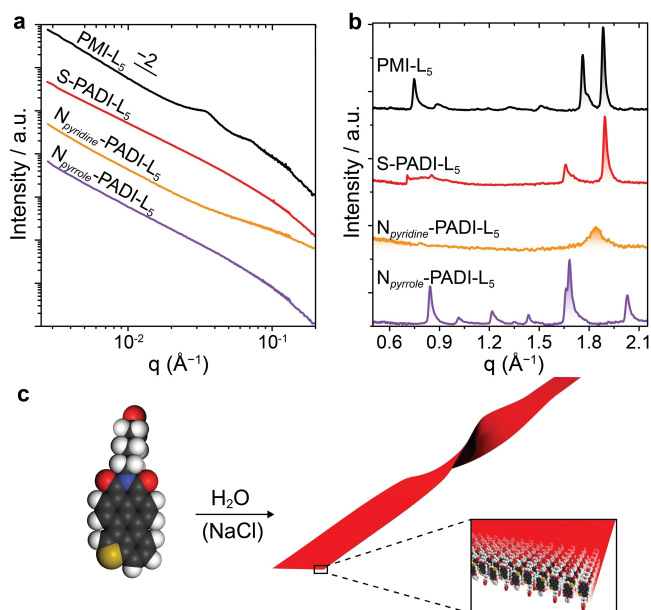


Figure 4. a) Solution small-angle X-ray scattering of self-assembled PADIs (10 mM with 50 mM aq. NaCl, annealed). b) Solution wide-angle X-ray scattering of self-assembled PADIs (10 mM with 50 mM aq. NaCl, annealed). c) Schematic representation of PADI supramolecular polymers in aqueous solutions in the presence of electrolytes for charge screening.

a methoxy substituent in the 9-position, which matches the increased dipole moment of the monomer.^[10c]

To confirm the formation of nanoribbons observed by solution X-ray scattering (for a schematic representation see Figure 4c), we used microscopy on thermally annealed liquid samples (confocal and atomic force microscopies) and on samples that were subsequently dried (transmission electron microscopy and selected area diffraction). Images of the solutions obtained with confocal laser-scanning microscopy (CLSM) showed the presence of nanoribbons in the PADI samples. PMI-L₅ (**1**) forms wider ribbons (Figure 5a), while S-PADI-L₅ (**2**) and N_{pyrrole}-PADI-L₅ (**4**) ribbons are narrower and tend to curl (observed as bright spots in Figure 5d,j). N_{pyridine}-PADI-L₅ (**3**), on the other hand, shows the presence of needle-like structures (Figure 5g). Transmission electron microscopy (TEM) and atomic force microscopy (AFM) confirm the ribbon-like morphology observed in confocal images, but with the following exceptions. S-PADI-L₅ (**2**) and N_{pyrrole}-PADI-L₅ (**4**) ribbons observed are rather short (Figures 5e,k) compared to CLSM images, presumably because drop-casting and treatment of the samples broke the curled ribbons into pieces observed by TEM and AFM microscopies. For N_{pyridine}-PADI-L₅ samples (**3**) (Figures 5h,i), we observe the prevalence of fibers and a sparse presence of short ribbons (only the ribbons are visible in CLSM, TEM shows both morphologies, while the fibers are clearly observed by AFM). The height profiles of the nanostructures measured by AFM reveal a height of approximately 2–3 nm for the supramolecular polymers (Supporting Information, Figure S63), which corresponds to a monolayer of the PADI molecules (as shown in the

schematic representation in Figure 4c). Finally, we used electron beam diffraction analysis (Supporting Information, Figures S64 and S65) to confirm the WAXS data (Figure 4b) and obtain the distinct unit cells for PADI ribbons. It is interesting to note that the (sparsely observed) short ribbons of **3** have crystalline features, as shown by the electron diffraction pattern (Supporting Information, Figure S64c), although Bragg reflections are not observed in bulk samples characterized by WAXS (Figure 4b).

Based on these experiments, we attribute the dipole moment as the main intermolecular interaction that drives the π - π antiparallel molecular packing (short axis *d*-spacing) and directs anisotropic polymerization of the nanostructures. Although the introduction of heterocycles is clearly responsible for notable changes in the morphology and crystallinity of the supramolecular polymers formed, we suggest the differences are mainly due to the molecular dipole moment of the monomers. Indeed, S-PADI-L₅ (**2**) and PMI-L₅ (**1**) display similar unit cells and similar dipole moments, although compound **2** has a tendency to curl, probably due to the supramolecular packing of the asymmetric molecules.^[10h] The N_{pyrrole}-PADI-L₅ (**4**) unit cell, as previously mentioned, matched that of a CH₃O-PMI-L₅ derivative,^[10c] and they both exhibit higher dipole moments relative to the PMI-L₅, which strongly favors an antiparallel arrangement of molecules.^[10h] The higher dipole moment of N_{pyrrole}-PADI-L₅ (**4**) compared to PMI-L₅ could also explain the formation of narrower ribbons due to the introduction of a repulsive component. Finally, the N_{pyridine}-PADI-L₅ (**3**) polymers, the overall molar mass of supramolecular polymers is low because the synergy of antiparallel attractive dipolar forces and π - π stacking is not provided by this chemical structure.

Conductivity of supramolecular polymers

We then investigated the effect of heterocyclic structure on bulk electrical conductivity (σ) of the PADI supramolecular polymers. The samples (10 mM, with 50 mM aq. NaCl and thermally annealed) were spin-coated onto SiO₂/Si substrates, followed by evaporation of thick gold contacts. Current-voltage (*I*-*V*) measurements were then carried out using the two-probe method (Figure 6a). The model PMI-L₅ (**1**) nanoribbons have a conductivity of $2.1 \times 10^{-5} \text{ Scm}^{-1}$, while the introduction of electron-poor and electron-rich nitrogen in N_{pyridine}-PADI-L₅ (**3**) and N_{pyrrole}-PADI-L₅ (**4**) does not result in large differences in thin film conductivities (5.1 and $3.4 \times 10^{-5} \text{ Scm}^{-1}$, respectively). Interestingly, the S-PADI-L₅ nanoribbons reveal a 20-fold higher conductivity ($4.1 \times 10^{-4} \text{ Scm}^{-1}$) compared to the PMI-L₅ (**1**) sample. In order to understand the influence of the heteroatom on charge transport properties, we focused on **1** and **2** since they have similar molecular packing and monomer properties. We considered the origin of the electrical conductivity difference between PMI-L₅ (**1**) and S-PADI-L₅ (**2**) by measuring the conductance of individual supramolecular ribbons polymers. Conductive atomic force microscopy (cAFM) measurements^[19] were carried out and *I*-*V* curves

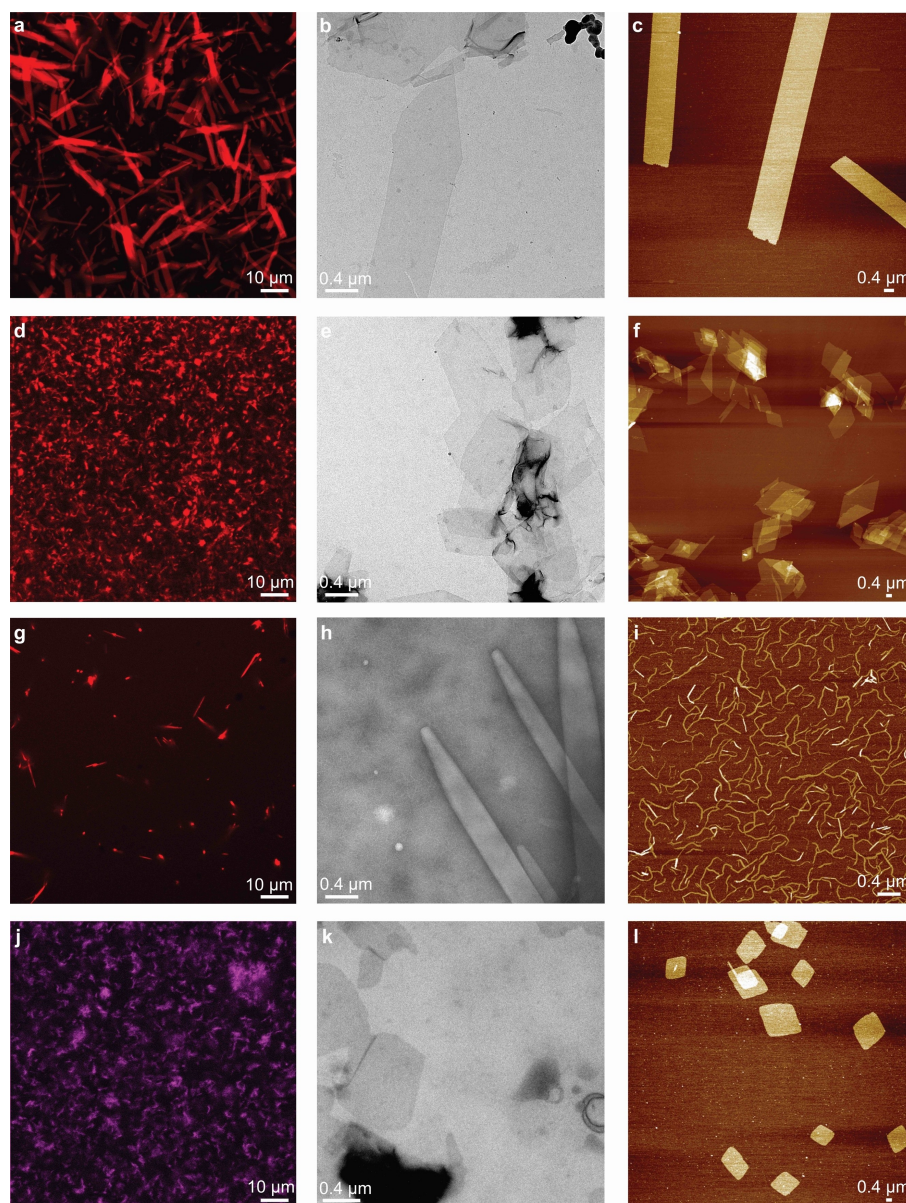


Figure 5. Micrographs of PADI nanostructures after thermal annealing in the presence of 50 mM aq. NaCl. From top to bottom: (a,b,c) PMI-L₅ **1**, (d,e,f) S-PADI-L₅ **2**, (g,h,i) N_{pyridine}-PADI-L₅ **3**, (j,k,l) N_{pyrrole}-PADI-L₅ **4**. (a,d,g,h) Confocal laser-scanning microscopy of PADI nanostructures. (b,e,h,k) TEM images of drop-cast samples of PADI nanostructures (from 10 mM solution with 50 mM aq. NaCl). (c,f,i,l) AFM height images of annealed PMI-L₅ and PADIs-L₅ (10 mM with 50 mM aq. NaCl) in fluid imaging mode.

were obtained at different points along the nanoribbon length (Figure 6d,e and Supporting Information Section 9). While the S-PADI-L₅ and PMI-L₅ nanostructures have similar widths, cAFM revealed that the S-PADI-L₅ (**2**) supramolecular polymers possess notably higher conductance compared to the PMI-L₅ (**1**) nanoribbons. The increased conductance is therefore likely due to short-range ordering within single nanoribbons, rather than the morphological differences between the nanostructures. We postulate that the benzene-to-thiophene substitution influences short-range interactions and is responsible for the increase in conductance at the single nanoribbon level. Indeed, sulfur-arene interactions are known to have a stabilizing effect and

have been attributed to the availability of empty 3d orbitals on sulfur and its enhanced polarizability.^[20] At present, however, we cannot exclude that there could be other contributions, such as the presence of defects or lattice distortions.^[4d,21]

Finally, the low conductivities from N-containing heterocyclic PADIs, N_{pyridine}-PADI-L₅ (**3**) and N_{pyrrole}-PADI-L₅ (**4**), could be ascribed either to the lower overall molar mass of supramolecular polymers (N_{pyridine}-PADI-L₅, **3**) or due to the large dipole moment which is known to cause transverse shifts and rotations between stacked molecules (N_{pyrrole}-PADI-L₅, **4**). Indeed, N_{pyrrole}-PADI-L₅, **4** crystalline polymers form similar unit cells as the previously reported 9-

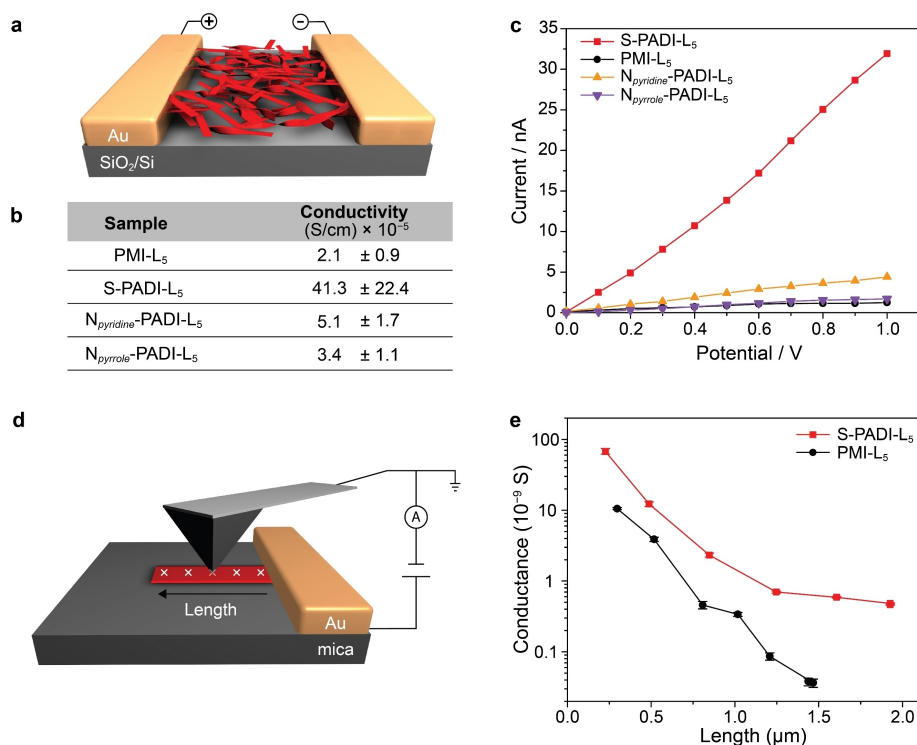


Figure 6. a) Schematic representation of the device employed to study the bulk conductivity. b) Conductivity values for the spin-coated PADI nanostructures. c) I–V traces for PADI nanostructures. d) Schematic representation for the conductive AFM (cAFM) measurements. e) Plot of the conductance of single S-PADI-L₅ and PMI-L₅ nanoribbons at different points along the nanoribbon length (as shown in panel e).

methoxy substituted PMI derivative,^[10c] with the significant distortions from the face-to-face antiparallel stacking resulting in small orbital overlaps,^[10c] thereby lowering conductivity across the nanostructures.

Conclusion

We have studied here the impact of heterocyclic substitutions on structure and properties in supramolecular polymers formed by chromophore amphiphiles. This approach has emerged as a useful tool to tailor optoelectronic and electrochemical properties, crystallization, aromaticity, and chemical stability of polycyclic aromatic hydrocarbons, but has not been systematically explored for aqueous supramolecular polymerization of polycyclic aromatic hydrocarbons. We found that substitution of dicarboximide monomers with electron-deficient rings such as pyridine led to molecules with weak dipole moments that tend to polymerize into non-crystalline nanofibers, due to decreased dipole-dipole interactions. Electron-rich heterocycles, such as pyrrole, yield molecules with strong ground state dipoles that form narrow ribbon-shaped crystalline supramolecular polymers. We propose that large changes to the dipole moment of the monomers yield supramolecular polymers with low electrical conductivity because of decreased overlap between stacked molecules, either due to lack of dipole-dipole interactions or introduction of a repulsive component. Interestingly, the introduction of a thiophene hetero-

cycle in the monomeric structure does not notably alter the supramolecular polymerization, but results in nanostructures with much higher electrical conductivity not predictable from monomeric properties. The increase of the conductivity is possibly due to enhanced dispersion interactions as a result of the presence of sulfur atoms.

The results point to the importance of heteroatom substitution on altering of monomeric molecular dipole moments, which impact the internal order within the polymeric assemblies. The conductivity of the supramolecular polymers formed are seemingly more dependent on short range interactions, which are not easily predicted from monomer properties. Overall, this work opens new possibilities to tailor monomers and the resulting supramolecular polymers into functional materials and their integration into organic optoelectronic devices.

Acknowledgements

This work was funded by the Center for Bio-Inspired Energy Science (CBES), an Energy Frontier Research Center funded by the U.S. Department of Energy, Office of Science, Basic Energy Sciences (DOE-BES) under award number DE-SC0000989. Use of the Advanced Photon Source (APS) was supported by the Basic Energy Sciences program of the U.S. Department of Energy, Office of Science, under Contract No. DE-AC02-06CH11357. Angle dependent X-ray experiments were performed at the

DuPont-Northwestern-Dow Collaborative Access Team (DND-CAT) located at Sector 5 of the APS. DND-CAT is supported by Northwestern University, E.I. DuPont de Nemours & Co., and the Dow Chemical Company. We thank the Biological Imaging Facility at Northwestern for the use of TEM equipment and the Electron Probe Instrumentation Center facilities of the Northwestern University Atomic and Nanoscale Characterization Experimental Center. This work made use of the IMSERC NMR and MS facilities at Northwestern University, which have received support from the Soft and Hybrid Nanotechnology Experimental (SHyNE) Resource (NSF ECCS-2025633), Northwestern University, the State of Illinois, and the International Institute for Nanotechnology (IIN). Conductivity measurements were completed in the NUFAB facility of Northwestern University's NUANCE Center, which has received support from the SHyNE Resource (NSF ECCS-2025633), the IIN, and Northwestern's MRSEC program (NSF DMR-1720139). The authors would also like to thank Mark Seniow for his help in preparing the schematics used in the manuscript.

Conflict of Interest

The authors declare no conflict of interest.

Data Availability Statement

The data that support the findings of this study are available from the corresponding author upon reasonable request.

Keywords: Chromophores · Doping · Nanostructures · Self-Assembly · Supramolecular Chemistry

- [1] a) J. M. Lehn, *Science* **1985**, 227, 849–856; b) T. Aida, E. W. Meijer, S. I. Stupp, *Science* **2012**, 335, 813–817; c) E. Busseron, Y. Ruff, E. Moulin, N. Giuseppone, *Nanoscale* **2013**, 5, 7098–7140; d) T. Brixner, R. Hildner, J. Köhler, C. Lambert, F. Würthner, *Adv. Energy Mater.* **2017**, 7, 1700236; e) P. K. Hashim, J. Bergueiro, E. W. Meijer, T. Aida, *Prog. Polym. Sci.* **2020**, 105, 101250; f) G. Ghosh, P. Dey, S. Ghosh, *Chem. Commun.* **2020**, 56, 6757–6769; g) O. Dumele, J. Chen, J. V. Passarelli, S. I. Stupp, *Adv. Mater.* **2020**, 32, 1907247.
- [2] a) M. R. Wasielewski, *Acc. Chem. Res.* **2009**, 42, 1910–1921; b) S. S. Babu, S. Prasanthkumar, A. Ajayaghosh, *Angew. Chem. Int. Ed.* **2012**, 51, 1766–1776; *Angew. Chem.* **2012**, 124, 1800–1810; c) S. Sengupta, F. Würthner, *Acc. Chem. Res.* **2013**, 46, 2498–2512; d) A. Jain, S. J. George, *Mater. Today* **2015**, 18, 206–214; e) S. Chen, P. Slattum, C. Wang, L. Zang, *Chem. Rev.* **2015**, 115, 11967–11998; f) M. Sun, K. Mullen, M. Yin, *Chem. Soc. Rev.* **2016**, 45, 1513–1528; g) P. S. Bols, H. L. Anderson, *Acc. Chem. Res.* **2018**, 51, 2083–2092; h) E. P. Bruckner, T. Curk, L. Đorđević, Z. Wang, Y. Yang, R. Qiu, A. J. Dannenhoffer, H. Sai, J. Kupferberg, L. C. Palmer, E. Luijten, S. I. Stupp, *ACS Nano* **2022**, 16, 8993–9003; i) O. Dumele, L. Đorđević, H. Sai, T. J. Cotey, M. H. Sangji, K. Sato, A. J. Dannenhoffer, S. I. Stupp, *J. Am. Chem. Soc.* **2022**, 144, 3127–3136.
- [3] a) A. L. Briseno, S. C. Mannsfeld, C. Reese, J. M. Hancock, Y. Xiong, S. A. Jenekhe, Z. Bao, Y. Xia, *Nano Lett.* **2007**, 7, 2847–2853; b) Z. Chen, V. Stepanenko, V. Dehm, P. Prins, L. D. Siebbeles, J. Seibt, P. Marquetand, V. Engel, F. Würthner, *Chem. Eur. J.* **2007**, 13, 436–449; c) X. Feng, V. Marcon, W. Pisula, M. R. Hansen, J. Kirkpatrick, F. Grozema, D. Andrienko, K. Kremer, K. Mullen, *Nat. Mater.* **2009**, 8, 421–426; d) J. C. Barnes, E. J. Dale, A. Prokofjevs, A. Narayanan, I. C. Gibbs-Hall, M. Juricek, C. L. Stern, A. A. Sarjeant, Y. Y. Botros, S. I. Stupp, J. F. Stoddart, *J. Am. Chem. Soc.* **2015**, 137, 2392–2399; e) Y. Sheng, W. Li, L. Xu, Y. Zhu, *Adv. Mater.* **2022**, 34, 2102354.
- [4] a) E. Krieg, M. M. Bastings, P. Besenius, B. Rybtchinski, *Chem. Rev.* **2016**, 116, 2414–2477; b) L. Zhang, S. Li, M. A. Squillaci, X. Zhong, Y. Yao, E. Orgiu, P. Samori, *J. Am. Chem. Soc.* **2017**, 139, 14406–14411; c) E. Krieg, A. Niazov-Elkan, E. Cohen, Y. Tsarfati, B. Rybtchinski, *Acc. Chem. Res.* **2019**, 52, 2634–2646; d) Y. Yao, L. Zhang, E. Orgiu, P. Samori, *Adv. Mater.* **2019**, 31, 1900599.
- [5] a) E. R. Draper, D. J. Adams, *Langmuir* **2019**, 35, 6506–6521; b) P. R. A. Chivers, D. K. Smith, *Nat. Rev. Mater.* **2019**, 4, 463–478; c) N. A. Sather, H. Sai, I. R. Sasselli, K. Sato, W. Ji, C. V. Synatschke, R. T. Zambrotta, J. F. Edelbrock, R. R. Kohlmeier, J. O. Hardin, J. D. Berrigan, M. F. Durstock, P. Mirau, S. I. Stupp, *Small* **2021**, 17, 2005743.
- [6] a) J. A. Lehrman, H. Cui, W. W. Tsai, T. J. Moyer, S. I. Stupp, *Chem. Commun.* **2012**, 48, 9711–9713; b) J. D. Tovar, *Acc. Chem. Res.* **2013**, 46, 1527–1537; c) E. R. Jira, K. Shmilovich, T. S. Kale, A. Ferguson, J. D. Tovar, C. M. Schroeder, *ACS Appl. Mater. Interfaces* **2020**, 12, 20722–20732; d) R. J. Hafner, D. Gorl, A. Sienkiewicz, S. Balog, H. Frauenrath, *Chem. Eur. J.* **2020**, 26, 9506–9517.
- [7] a) E. R. Draper, B. Dietrich, D. J. Adams, *Chem. Commun.* **2017**, 53, 1864–1867; b) S. Biswas, M. Kumar, A. M. Levine, I. Jimenez, R. V. Ulijn, A. B. Braunschweig, *Chem. Sci.* **2020**, 11, 4239–4245.
- [8] a) M. Kumar, D. Sementa, V. Narang, E. Riedo, R. V. Ulijn, *Chem. Eur. J.* **2020**, 26, 8372–8376; b) C. Berdugo, S. K. Nalluri, N. Javid, B. Escuder, J. F. Miravet, R. V. Ulijn, *ACS Appl. Mater. Interfaces* **2015**, 7, 25946–25954; c) M. Kumar, N. L. Ing, V. Narang, N. K. Wijerathne, A. I. Hochbaum, R. V. Ulijn, *Nat. Chem.* **2018**, 10, 696–703.
- [9] a) D. Gorl, X. Zhang, V. Stepanenko, F. Würthner, *Nat. Commun.* **2015**, 6, 7009; b) J. J. Walsh, J. R. Lee, E. R. Draper, S. M. King, F. Jäckel, M. A. Zwijnenburg, D. J. Adams, A. J. Cowan, *J. Phys. Chem. C* **2016**, 120, 18479–18486; c) E. R. Draper, J. R. Lee, M. Wallace, F. Jäckel, A. J. Cowan, D. J. Adams, *Chem. Sci.* **2016**, 7, 6499–6505; d) E. R. Draper, B. J. Greeves, M. Barrow, R. Schweins, M. A. Zwijnenburg, D. J. Adams, *Chem* **2017**, 2, 716–731; e) A. Sorrenti, J. Leira-Iglesias, A. Sato, T. M. Hermans, *Nat. Commun.* **2017**, 8, 15899; f) A. Wang, L. Cui, S. Debnath, Q. Dong, X. Yan, X. Zhang, R. V. Ulijn, S. Bai, *ACS Appl. Mater. Interfaces* **2017**, 9, 21390–21396; g) E. R. Draper, L. J. Archibald, M. C. Nolan, R. Schweins, M. A. Zwijnenburg, S. Sproules, D. J. Adams, *Chem. Eur. J.* **2018**, 24, 4006–4010; h) M. A. Martínez, E. E. Greciano, J. Cuéllar, J. M. Valpuesta, L. Sánchez, *Nanomaterials* **2021**, 11, 1457.
- [10] a) A. S. Weingarten, R. V. Kazantsev, L. C. Palmer, M. McClendon, A. R. Koltanow, A. P. Samuel, D. J. Kiebal, M. R. Wasielewski, S. I. Stupp, *Nat. Chem.* **2014**, 6, 964–970; b) A. S. Weingarten, R. V. Kazantsev, L. C. Palmer, D. J. Fairfield, A. R. Koltanow, S. I. Stupp, *J. Am. Chem. Soc.* **2015**, 137, 15241–15246; c) B. Harutyunyan, A. Dannenhoffer, S. Kewalramani, T. Aytun, D. J. Fairfield, S. I. Stupp, M. J. Bedzyk, *J. Phys. Chem. C* **2017**, 121, 1047–1054; d) R. V. Kazantsev, A. J. Dannenhoffer, A. S. Weingarten, B. T. Phe-

- lan, B. Harutyunyan, T. Aytun, A. Narayanan, D. J. Fairfield, J. Boekhoven, H. Sai, A. Senesi, P. I. O'Dogherty, L. C. Palmer, M. J. Bedzyk, M. R. Wasielewski, S. I. Stupp, *J. Am. Chem. Soc.* **2017**, *139*, 6120–6127; e) R. V. Kazantsev, A. Dannenhoffer, T. Aytun, B. Harutyunyan, D. J. Fairfield, M. J. Bedzyk, S. I. Stupp, *Chem* **2018**, *4*, 1596–1608; f) A. S. Weingarten, A. J. Dannenhoffer, R. V. Kazantsev, H. Sai, D. Huang, S. I. Stupp, *J. Am. Chem. Soc.* **2018**, *140*, 4965–4968; g) A. Dannenhoffer, H. Sai, D. Huang, B. Nagasing, B. Harutyunyan, D. J. Fairfield, T. Aytun, S. M. Chin, M. J. Bedzyk, M. Olvera de la Cruz, S. I. Stupp, *Chem. Sci.* **2019**, *10*, 5779–5786; h) H. Sai, G. C. Lau, A. J. Dannenhoffer, S. M. Chin, L. Đorđević, S. I. Stupp, *Nano Lett.* **2020**, *20*, 4234–4241; i) A. Dannenhoffer, H. Sai, E. P. Bruckner, L. Đorđević, A. Narayanan, Y. Yang, X. Ma, L. C. Palmer, S. I. Stupp, *Chem* **2023**, *9*, 170–180.
- [11] a) K. Shoyama, M. Mahl, S. Seifert, F. Würthner, *J. Org. Chem.* **2018**, *83*, 5339–5346; b) K. Shoyama, M. Mahl, M. A. Niyas, M. Ebert, V. Kachler, C. Keck, F. Würthner, *J. Org. Chem.* **2020**, *85*, 142–149; c) W. Jiang, Z. Wang, *J. Am. Chem. Soc.* **2022**, *144*, 14976–14991.
- [12] a) M. Stępień, E. Gońka, M. Żyła, N. Sprutta, *Chem. Rev.* **2017**, *117*, 3479–3716; b) M. Hirai, N. Tanaka, M. Sakai, S. Yamaguchi, *Chem. Rev.* **2019**, *119*, 8291–8331; c) S. Hayakawa, A. Kawasaki, Y. Hong, D. Uraguchi, T. Ooi, D. Kim, T. Akutagawa, N. Fukui, H. Shinokubo, *J. Am. Chem. Soc.* **2019**, *141*, 19807–19816; d) U. H. F. Bunz, J. Freudenberg, *Acc. Chem. Res.* **2019**, *52*, 1575–1587; e) N. Biot, D. Bonifazi, *Coord. Chem. Rev.* **2020**, *413*, 213243; f) S. M. Suresh, E. Duda, D. Hall, Z. Yao, S. Bagnich, A. M. Z. Slawin, H. Bassler, D. Beljonne, M. Buck, Y. Olivier, A. Kohler, E. Zysman-Colman, *J. Am. Chem. Soc.* **2020**, *142*, 6588–6599; g) T. Okamoto, C. P. Yu, C. Mitsui, M. Yamagishi, H. Ishii, J. Takeya, *J. Am. Chem. Soc.* **2020**, *142*, 9083–9096; h) J. E. Barker, J. J. Dressler, A. Cardenas Valdivia, R. Kishi, E. T. Strand, L. N. Zakharov, S. N. MacMillan, C. J. Gomez-Garcia, M. Nakano, J. Casado, M. M. Haley, *J. Am. Chem. Soc.* **2020**, *142*, 1548–1555; i) S. N. Intorp, M. Hodecker, M. Muller, O. Tverskoy, M. Rosenkranz, E. Dmitrieva, A. A. Popov, F. Rominger, J. Freudenberg, A. Dreuw, U. H. F. Bunz, *Angew. Chem. Int. Ed.* **2020**, *59*, 12396–12401; *Angew. Chem.* **2020**, *132*, 12496–12501; j) L. Đorđević, C. Valentini, N. Demitri, C. Meziere, M. Allain, M. Salle, A. Folli, D. Murphy, S. Manas-Valero, E. Coronado, D. Bonifazi, *Angew. Chem. Int. Ed.* **2020**, *59*, 4106–4114; *Angew. Chem.* **2020**, *132*, 4135–4143; k) J. Lawrence, G. C. Sossio, L. Đorđević, H. Pinfold, D. Bonifazi, G. Costantini, *Nat. Commun.* **2020**, *11*, 2103; l) L. Đorđević, D. Milano, N. Demitri, D. Bonifazi, *Org. Lett.* **2020**, *22*, 4283–4288; m) F. Hernandez-Culebras, M. Melle-Franco, A. Mateo-Alonso, *Angew. Chem. Int. Ed.* **2022**, *61*, e202205018; *Angew. Chem.* **2022**, *134*, e202205018; n) A. Borissov, Y. K. Maurya, L. Moshniha, W. S. Wong, M. Zyla-Karwowska, M. Stepień, *Chem. Rev.* **2022**, *122*, 565–788; o) M. Martínez-Abadía, R. K. Dubey, M. Fernández, M. Martín-Arroyo, R. Aguirresarobe, A. Saeki, A. Mateo-Alonso, *Chem. Sci.* **2022**, *13*, 10773–10778.
- [13] a) X. Y. Wang, X. Yao, A. Narita, K. Mullen, *Acc. Chem. Res.* **2019**, *52*, 2491–2505; b) J. A. Berrocal, M. F. J. Mabeoone, M. Garcia Iglesias, A. Huizinga, E. W. Meijer, A. R. A. Palmans, *Chem. Commun.* **2019**, *55*, 14906–14909; c) T. Aida, E. W. Meijer, *Isr. J. Chem.* **2020**, *60*, 33–47; d) B. Adelizzi, P. Chidchob, N. Tanaka, B. A. G. Lamers, S. C. J. Meskers, S. Ogi, A. R. A. Palmans, S. Yamaguchi, E. W. Meijer, *J. Am. Chem. Soc.* **2020**, *142*, 16681–16689; e) Z. Liu, S. Fu, X. Liu, A. Narita, P. Samori, M. Bonn, H. I. Wang, *Adv. Sci.* **2022**, *9*, 2106055.
- [14] a) S. Seifert, K. Shoyama, D. Schmidt, F. Würthner, *Angew. Chem. Int. Ed.* **2016**, *55*, 6390–6395; *Angew. Chem.* **2016**, *128*, 6500–6505; b) S. Seifert, D. Schmidt, F. Würthner, *Org. Chem. Front.* **2016**, *3*, 1435–1442; c) S. Seifert, D. Schmidt, K. Shoyama, F. Würthner, *Angew. Chem. Int. Ed.* **2017**, *56*, 7595–7600; *Angew. Chem.* **2017**, *129*, 7703–7708; d) K. Shoyama, D. Schmidt, M. Mahl, F. Würthner, *Org. Lett.* **2017**, *19*, 5328–5331; e) D. Uersfeld, S. Stappert, C. Li, K. Müllen, *Adv. Synth. Catal.* **2017**, *359*, 4184–4189; f) M. Mahl, K. Shoyama, J. Ruhe, V. Grande, F. Würthner, *Chem. Eur. J.* **2018**, *24*, 9409–9416; g) H. Zhylitskaya, M. Stępień, *Org. Chem. Front.* **2018**, *5*, 2395–2414; h) K. Shoyama, F. Würthner, *J. Am. Chem. Soc.* **2019**, *141*, 13008–13012; i) B. Pigulski, M. Ximenis, K. Shoyama, F. Würthner, *Org. Chem. Front.* **2020**, *7*, 2925–2930; j) R. Renner, M. Stolte, F. Würthner, *ChemistryOpen* **2020**, *9*, 32–39; k) X. Zhao, X. Chen, Z. Yuan, H. Zhang, G. Luo, Y. Hu, Y. Chen, *Dyes Pigm.* **2020**, *173*, 107930; l) B. Mahlmeister, M. Mahl, H. Reichelt, K. Shoyama, M. Stolte, F. Würthner, *J. Am. Chem. Soc.* **2022**, *144*, 10507–10514; m) B. Pigulski, K. Shoyama, M. J. Sun, F. Würthner, *J. Am. Chem. Soc.* **2022**, *144*, 5718–5722; n) M. Mahl, M. A. Niyas, K. Shoyama, F. Würthner, *Nat. Chem.* **2022**, *14*, 457–462.
- [15] A. J. Dannenhoffer, H. Sai, B. Harutyunyan, A. Narayanan, N. E. Powers-Riggs, A. N. Edelbrock, J. V. Passarelli, S. J. Weigand, M. R. Wasielewski, M. J. Bedzyk, L. C. Palmer, S. I. Stupp, *Nano Lett.* **2021**, *21*, 3745–3752.
- [16] Deposition Number 2192609 (for S-PADI-L₅, **2**) contains the supplementary crystallographic data for this paper. These data are provided free of charge by the joint Cambridge Crystallographic Data Centre and Fachinformationszentrum Karlsruhe Access Structures service.
- [17] a) A. Sorrenti, J. Leira-Iglesias, A. J. Markvoort, T. F. A. de Greef, T. M. Hermans, *Chem. Soc. Rev.* **2017**, *46*, 5476–5490; b) J. Matern, Y. Dorca, L. Sanchez, G. Fernandez, *Angew. Chem. Int. Ed.* **2019**, *58*, 16730–16740; *Angew. Chem.* **2019**, *131*, 16884–16895; c) M. Wehner, F. Würthner, *Nat. Chem. Rev.* **2020**, *4*, 38–53.
- [18] N. J. Hestand, R. V. Kazantsev, A. S. Weingarten, L. C. Palmer, S. I. Stupp, F. C. Spano, *J. Am. Chem. Soc.* **2016**, *138*, 11762–11774.
- [19] J. M. Mativetsky, Y.-L. Loo, P. Samorì, *J. Mater. Chem. C* **2014**, *2*, 3118–3128.
- [20] a) E. A. Meyer, R. K. Castellano, F. Diederich, *Angew. Chem. Int. Ed.* **2003**, *42*, 1210–1250; *Angew. Chem.* **2003**, *115*, 1244–1287; b) W. B. Motherwell, R. B. Moreno, I. Pavlakos, J. R. T. Arendorf, T. Arif, G. J. Tizzard, S. J. Coles, A. E. Aliev, *Angew. Chem. Int. Ed.* **2018**, *57*, 1193–1198; *Angew. Chem.* **2018**, *130*, 1207–1212.
- [21] Z. Chai, A. Childress, A. A. Busnaina, *ACS Nano* **2022**, *16*, 17641–17686.

Manuscript received: October 11, 2022

Accepted manuscript online: March 2, 2023

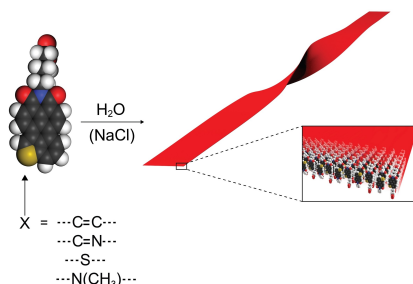
Version of record online: ■■■■■

Research Articles

Supramolecular Polymers

L. Đorđević, H. Sai, Y. Yang, N. A. Sather,
L. C. Palmer, S. I. Stupp* — **e202214997**

Heterocyclic Chromophore Amphiphiles
and their Supramolecular Polymerization



Heterocycles have been introduced into the structure of the model perylene monoimide chromophore amphiphile to afford monomers that undergo supramolecular polymerization in water but have different conductivities. The heterocycles alter the monomeric molecular dipole moments, which impacts the internal order within the polymeric assemblies. The conductivity of the supramolecular polymers formed are seemingly dependent on short-range interactions.